



Unravelling the role of Co in mixed Ni-Co oxygen carriers/catalysts for H₂ production via sorption enhanced steam methane reforming coupled with chemical looping

Theodoros Papalas ^a, Andy N. Antzaras ^{a,*}, Angeliki A. Lemonidou ^{a,b}

^a Department of Chemical Engineering, Aristotle University of Thessaloniki, University Campus, 54124 Thessaloniki, Greece

^b Chemical Process & Energy Resource Institute, CPERI/CERTH, Thermi, Thessaloniki 57001, Greece



ARTICLE INFO

Keywords:

Sorption enhanced hydrogen production
Process intensification
CO₂ capture
Chemical looping
Ni-Co oxygen carrier

ABSTRACT

Coupling steam methane reforming with calcium and chemical looping comprises an energy efficient pathway for intensified high-purity H₂ production. CaO carbonation enables the in-situ CO₂ removal, along with elevated CH₄ conversion and H₂ yield in a single step, while the energy demand of calcination is covered by the oxygen carrier oxidation. This work evaluated bimetallic Ni-Co oxygen carriers for their performance under the intensified reforming conditions, when applied as a mechanical mixture with a CaO-based material with a molar ratio of Ni-Co oxides to CaO of 0.5. In the reforming stage, the oxygen carrier underwent reduction to form a Ni-Co alloy, serving as catalyst for H₂ production with ~94% purity and ~90% yield at 650 °C. The subsequent oxidation of the Ni-Co oxygen carrier under air covered adiabatically ~40% of the calcination energy demand, which is ~42% higher compared to a monometallic Ni-based material. The better activity of Ni-Co materials was ascribed to Co, which enhances the oxidation kinetics, as confirmed via in-situ X-ray diffraction.

1. Introduction

The on-going instability of the global energy sector and the extensive consumption of fossil fuels to satisfy the global demand for energy have nourished concerns related to energy security and climate change. H₂ comprises an important pillar of the energy sector, with its demand being determined primarily by its application as raw material in chemicals, petrochemicals, oil refineries and steel industries. In pursuit of attaining net zero emissions by 2050, H₂ demand as an energy carrier is expected also to grow in several other parts of the energy sector, such as transport, buildings and electricity generation, contributing up to 10% of the total energy consumption [1–3]. However, expanding the use of H₂ is hindered by its nature as secondary energy source derived nowadays mostly from fossil fuels, such as natural gas and coal. More specifically, steam methane reforming (SMR) is the leading industrial pathway for H₂ production, which is deemed as energy intensive and environmentally harmful, due to the high endothermicity and harsh operating conditions of the reformer (high temperatures and pressures of 800–900 °C and 20–30 atm). Another drawback is related to the thermodynamic limitations of reactions taking place in the reformer, which renders essential the addition of reaction and purification steps

downstream (e.g. water gas shift reactors and pressure swing adsorption units). Global efforts target to alleviate these issues by developing technologies (e.g. water electrolysis) based entirely on renewable sources. However, their increased levelised production costs and the lack of abundant renewable electricity will sustain the primacy of steam reforming for the coming years, thereby rendering the alleviation of its problems critical [4–6].

Process intensification has been recognized as a promising approach toward reducing the production steps and minimizing the energy requirements of industrial methods. The development of intensified reforming routes could allow H₂ derived from natural gas to continue playing a key role for the energy transition period [7]. One of the most studied intensification concepts is the Sorption Enhanced Steam Methane Reforming (SE-SMR), which employs a solid CO₂ capture material, such as CaO, to in-situ capture CO₂ during its production. The removal of CO₂ results in a shift toward a new thermodynamic equilibrium, according to Le Chatelier's principle. This enables for elevated CH₄ conversion and production of H₂ with higher yield and purity in a single step operating under milder temperatures (600–650 °C) compared to conventional reforming. Moreover, the energy released from the exothermic CaO carbonation is covering in-situ the heat

* Corresponding author.

E-mail address: aantzara@cheng.auth.gr (A.N. Antzaras).

demand of reforming, achieving almost autothermal operation [8–10]. Eventually, the CO_2 capture material reaches saturation, no longer attaining efficient CO_2 removal, thereby necessitating calcination in a separate reactor. When conducted under a CO_2 atmosphere to isolate a pure CO_2 stream for sequestration, CaCO_3 decomposition occurs at elevated temperatures (≥ 900 °C) and with high energy demand [11,12]. Several methods have been proposed to intensify this step, such as solar heating [13,14], in-situ conversion of CO_2 to high-value products [15,16] and the coupling with chemical looping [17–20].

Regarding the latter concept, Lyon and Cole proposed the introduction of a second chemical loop in SE-SMR leading to a hybrid process known as Sorption Enhanced Chemical Looping Steam Methane Reforming (SE-CL-SMR). The latter targets to meet in-situ the energy demand of calcination via the oxidation of an oxygen carrier (OC), such as NiO [17]. Similarly to the Ca-looping between oxide and carbonate forms, the OC undergoes continuous redox cycles, with reduction taking place in the reformer [19], for the reduced OC to serve as catalyst in the H_2 -producing reactions [21]. Over the years, the scientific community has studied various intensified reforming concepts that combine calcium and chemical looping [22–29]. Our group has also studied steam reforming coupled with Ca-Ni looping, including thermodynamic analysis [19], reactor design [30], material synthesis [31–34] and experimental demonstration [34–36].

The characteristics of the CaO -based material and OC comprise fundamental pillar for attaining high-purity H_2 generation in the reforming stage, while adjusting the ratio of the two materials is considered as one of the most important aspects for efficiently coupling the calcination and oxidation reactions. Increasing the NiO/CaO ratio can lead to even autothermal operation of CaCO_3 decomposition. A drawback though is the lower H_2 production yield, due to the consumption of higher amount of CH_4 and/or H_2 for OC reduction in the reforming stage [19,35]. Except from the mixing ratio, tailoring the structure of the CaO -based sorbent and OC can also affect the efficiency of the process. With regard to the OC, intermixing Ni with another metal can improve the catalytic and redox properties of the material [37–39]. Most literature studies that combine reforming with calcium and chemical looping in a single process [26,28,29,35] apply monometallic OCs, with the work of Fermo et al. comprising the only study that used a Pd-doped Ni-Co OC [27]. However, this work focused only on the beneficial effect of Pd on reforming, without providing insight on how the energy demand for calcination changes between polymetallic and monometallic materials. Hence, it is still unclear in open literature whether the partial substitution of Ni with another metal can be beneficial for the reforming and calcination/oxidation stages.

Our previous work dealt with bimetallic OCs with Ni-Co monoxides as active phase. Upon reduction, Ni-Co alloys were formed which retained high reforming catalytic activity when applying a low Co content (atomic $\text{Co}/(\text{Co}+\text{Ni}) \leq 0.20$). Co addition was found to improve the oxidation kinetics of OCs when tested under consecutive redox cycles in a thermogravimetric analyzer. These aspects are essential for high-purity H_2 production and for reduced calcination energy demand in SE-CL-SMR. Thus, this study serves as a continuation of our previous work and applies the developed bimetallic OCs in the intensified process. By conducting fixed bed reactor experiments, the aim was to investigate for the first time the role of Co in the coupling of calcination and oxidation reactions and to optimize the efficiency of SE-CL-SMR.

2. Experimental section

2.1. Synthesis of materials

A sol-gel auto-combustion method was followed for the synthesis of OCs with 40 wt% of Ni- and Co-based oxides and 60 wt% ZrO_2 . OCs were prepared with nitrate salt precursors and citric acid as combustion agent and consisted of a monometallic Ni-based material (denoted as Ni-Zr_{SG}) and two bimetallic ones with $\text{Co}/(\text{Ni}+\text{Co})$ atomic ratios of 0.12 and 0.20

($\text{Ni}_{0.88}\text{Co}_{0.12}\text{-Zr}$ and $\text{Ni}_{0.80}\text{Co}_{0.20}\text{-Zr}$ respectively). More details for the sol-gel synthesis can be found in our previous studies [34,40]. A monometallic Ni-based OC was also prepared via wet impregnation of Ni on a commercial ZrO_2 support (Ni-Zr_{WI}). This material was used in our previous SE-CL-SMR experiments [32,36] and was applied for comparison reasons. A synthetic CO_2 sorbent with 66 wt% CaO and 34 wt% CaZrO_3 composition was prepared via a sol-gel auto-combustion method [31], similar to the one applied for OCs. The final materials after calcination were pelletized, crushed and sieved to obtain a particle size between 180 and 355 μm .

2.2. Performance evaluation under SE-CL-SMR conditions

Sorption enhanced chemical looping steam methane reforming experiments were carried out at atmospheric pressure in a bench-scale continuous flow unit. A detailed description of the unit along with a representative scheme can be found in the [Supplementary material](#) (Fig. S1). A quartz reactor was loaded with 8 g of a mechanical mixture of an OC and a CaO -based material in appropriate quantities (mass ratio of OC to CaO -based material of ~ 1.1) to achieve a molar ratio of Ni- and Co-based oxides to CaO equal to 0.5 ($\text{Ni}_{(1-x)}\text{Co}_x\text{O}/\text{CaO}$ with x referring to the $\text{Co}/(\text{Co}+\text{Ni})$ ratio). Temperature was initially increased to 800 °C under air to remove CO_2 and H_2O that were captured from CaO during exposure in the atmosphere. The reactor was then cooled down to 650 °C and the gas feedstock was changed to a mixture of $\text{H}_2\text{O}/\text{CH}_4$ (100 ml/min, S/C = 3, GHSV = 215 h^{-1}) to initiate the H_2 production stage (rendered as *reduction/reforming/carbonation stage*), which is composed of the OC reduction, SMR, WGS and CaO carbonation reactions. Once the CO_2 capture material approached saturation, a purging step with He flow followed for ~ 3 min. The inlet gas was then switched to an oxidizing agent for the next reaction series (defined as *calcination/oxidation stage*) to occur. Starting from 650 °C and without providing external heating, the oxidizing agent provoked the re-oxidation of the OC and the partial CaCO_3 decomposition. After completing the OC oxidation, external heat was provided to increase the temperature of the reactor up to 800 °C and carry out the decomposition of the remaining CaCO_3 . A parametric evaluation was performed for the operation of the *calcination/oxidation stage*, which included the type of the oxidizing agent (air or pure O_2) and the GHSV (250–2000 h^{-1}) of the inlet flow. Temperature was then reduced to 650 °C under He flow to initiate the next *reduction/reforming/carbonation stage*, while the procedure described above was repeated for a total of 22 cycles to evaluate the stability of the materials. The methodology followed to analyse all results obtained from the SE-CL-SMR experiments is described in detail in the [Supplementary material](#).

2.3. Post-reaction characterization

Used materials after 22-cycle SE-CL-SMR experiments were characterized via various techniques to determine the effect of reaction tests on their structural properties. *Ex-situ* X-Ray Diffraction (XRD) analysis was conducted to check for alterations in the crystal structure, while *in-situ* XRD was also carried out to describe the effect of Co addition on the re-oxidation reaction. X-ray Photoelectron Spectroscopy (XPS) was performed to uncover the composition of the surface. Changes in the redox properties were examined via Temperature Programmed Reduction (TPR) with H_2 and Temperature Programmed Oxidation (TPO), while the latter quantified also carbon deposited after tests. A detailed description of all methods is available in the [Supplementary material](#).

3. Results and discussion

3.1. Performance of bimetallic OC in the hydrogen production stage

OCs should display high oxygen transfer capacity and catalytic activity for SMR in their reduced state for them to be suitable for

application in SE-CL-SMR process. Our previous work on the bimetallic Ni-Co OCs applied in this study proved that Co addition with low Co/(Ni+Co) ratio (≤ 0.20) could provide high oxygen transfer capacity, adequate reforming catalytic activity after reduction and enhanced kinetics of re-oxidation [40].

Fig. 1 illustrates the results obtained in the *reduction/reforming/carbonation stage* of a SE-CL-SMR experiment, in the presence of $\text{Ni}_{0.80}\text{Co}_{0.20}\text{-Zr}$ in mechanical mixture with the CaO-based material. The *reduction/reforming/carbonation stage* was conducted at 650°C , with S/C ratio of 3, GHSV = 215 h^{-1} and molar ratio of Ni- and Co-based oxides to active CaO of 0.5. Figs. 1B and 1C, which refer to the composition (on dry basis) of the gas exiting the reactor and the CH_4 conversion and H_2 yield respectively, can be divided into three distinct regimes. In the initial regime, which is referred as pre-breakthrough regime (Pre-BT), the efficient activity of the CO_2 capture material favored the reforming and WGS reactions toward products formation, allowing for $\sim 95\%$ CH_4 conversion and H_2 production with $\sim 94\%$ purity. The H_2 yield was lower ($\sim 84\%$) at the beginning of this regime, before reaching higher values ($\sim 90\%$) after ~ 10 min of reaction. The lower initial yield revealed the OC reduction by CH_4 and/or generated syngas, toward the formation of Ni-Co alloy, which then acted as catalyst for reforming and WGS reactions. The subsequent yield increase suggested that reduction was completed early in the Pre-BT regime, in accordance with literature [35,41], thereby enhancing CH_4 selectivity toward reforming and leading to a stable production of $\sim 0.98\text{ mmol H}_2/\text{min/g}$ of reduced OC. The attained CH_4 conversion and H_2 yield after the completion of OC reduction referred to the equilibrium of SE-SMR process (dashed lines of Fig. 1C) for the respective operating conditions (650°C , S/C=3, in the presence of available CaO). The high-purity H_2 generation is a result of the synergy of the CO_2 capture ability of the CaO-based material and the high catalytic activity of the formed Ni-Co alloy with Co/(Ni+Co) ratio

of 0.20, with the latter agreeing with the results of the conventional SMR experiments of our previous work [40]. Eventually, CaO conversion reached high values after ~ 50 min, which provoked the transition to the breakthrough (BT) regime, as proven by the gradual increase of CH_4 , CO and CO_2 concentrations and the decrease of H_2 purity. Finally, the post-breakthrough (Post-BT) began once the CO_2 capture material reached saturation and no longer intensified the H_2 production, while the CH_4 conversion and H_2 yield corresponded to the equilibrium of conventional SMR (650°C , S/C=3, absence of available CaO).

The aforementioned profile resembles the one obtained in sorption-enhanced reforming experiments with a Ni-based OC [29,35], proving that both monometallic and bimetallic OCs attain high H_2 production in the *reduction/reforming/carbonation stage*. It should be mentioned that the implementation of this process at industrial scale would require for the duration of this stage to end before the breakthrough, so as to fully capture the CO_2 , thus intensifying the H_2 production at maximum rate and generate a high purity H_2 stream over time. Therefore, for all experiments described below, the *reduction/reforming/carbonation stage* was ended before reaching the breakthrough of carbonation, attained by monitoring the CO_2 signal via the gas analyser with 2.5% cutoff.

3.2. Performance of oxygen carriers in the calcination/oxidation stage

After the end of the *reduction/reforming/carbonation stage*, the gas flow switched to air, which triggered a sharp temperature increase (Fig. 2B), as monitored by the three thermocouples in the axial direction, due to the exothermic OC oxidation. This temperature rise was initially observed in the upper part of the material bed and then it gradually shifted toward the bottom of the reactor in parallel with the reaction front. After completion of OC oxidation (~ 8 min), the

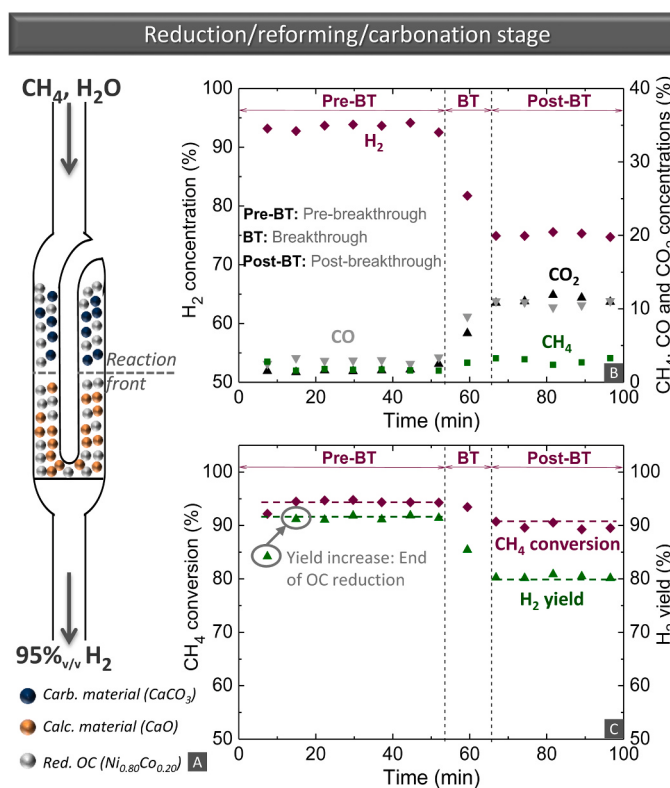


Fig. 1. (A) Reactor scheme of the reduction/reforming/carbonation stage of SE-CL-SMR, (B) gas product concentration, (C) CH_4 conversion and H_2 yield versus time when using $\text{Ni}_{0.80}\text{Co}_{0.20}\text{-Zr}$ as OC ($T = 650^\circ\text{C}$, S/C = 3, GHSV = 215 h^{-1} , molar $\text{Ni}_{0.80}\text{Co}_{0.20}\text{O}/\text{CaO} = 0.5$). Dashed lines of Fig. 1C refer to equilibrium.

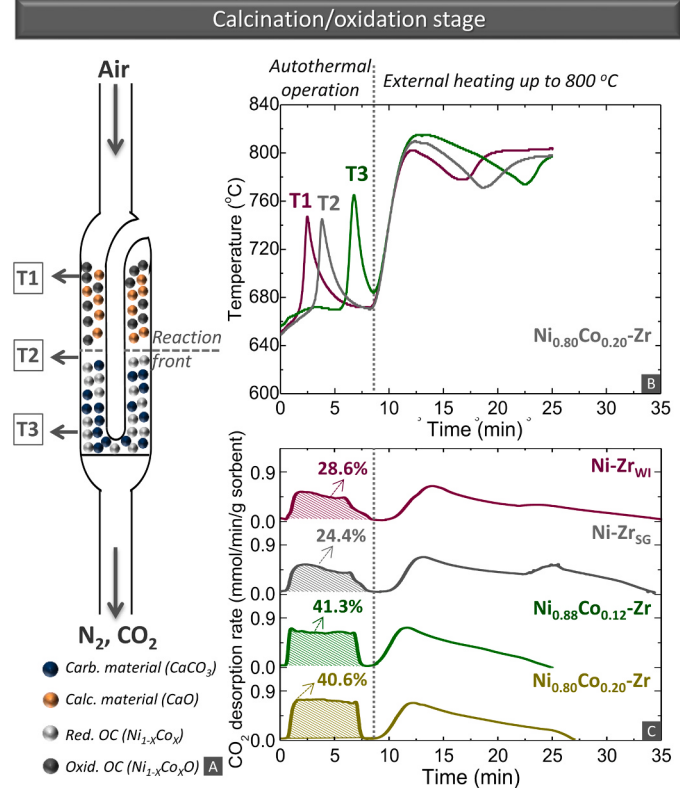


Fig. 2. (A) Reactor scheme of the calcination/oxidation stage of SE-CL-SMR, (B) temperature versus time when using $\text{Ni}_{0.80}\text{Co}_{0.20}\text{-Zr}$ as OC and (C) CO_2 desorption rate versus time for four experiments with different OCs ($T = 650\rightarrow 800^\circ\text{C}$, GHSV = 430 h^{-1} for Ni-Zr_{WI} , GHSV = 500 h^{-1} for other OCs, molar $\text{Ni}_{(1-x)}\text{Co}_x\text{O}/\text{CaO} = 0.5$).

temperature dropped close to its initial value and external heat was supplied to complete the decomposition of remaining CaCO_3 . In this regime, the endothermic calcination front also moved along the material length, since building high CO_2 partial pressures in the upper part, hindered calcination at lower layers of the bed. The position of the reaction front over time was indicated by the temperature drop recorded by each thermocouple.

The autothermal operation and external heating regimes can be also observed in the CO_2 outlet flow as a function of time in the *calcination/oxidation stage*. Fig. 2C presents the CO_2 release profiles and the autothermicity degree (AD_{exp}) calculated from Eq. (S4) of [Supplementary Material](#)) in four SE-CL-SMR experiments conducted with different OC materials. Ni-Zr_{WI} attained an AD_{exp} equal to 28.6%, which is in agreement with our previous results [35,36], while the use of Ni-Zr_{SG} led to a slightly lower AD_{exp} (24.4%), implying that the different synthesis technique does not have a major influence. Despite the same applied conditions and OC to CaO ratio in all experiments, in the presence of $\text{Ni}_{0.88}\text{Co}_{0.12}\text{-Zr}$ and $\text{Ni}_{0.80}\text{Co}_{0.20}\text{-Zr}$, a higher autothermicity was attained (41.3% and 40.6% respectively). This result provides a preliminary answer on the main research question posed in this work, since the application of bimetallic OCs was found beneficial for the SE-CL-SMR process, while the $\text{Co}/(\text{Ni}+\text{Co})$ atomic ratio of 0.12 and 0.20 did not seem to have any difference in the AD_{exp} attained. The total duration of the *calcination/oxidation stage* was shorter for bimetallic materials (~ 27 min) compared to monometallic ones (~ 35 min), due to the higher extent of autothermal calcination attained in the fast OC re-oxidation regime.

Another difference between the performance of OCs concerns the temperature profile, since the maximum temperature recorded in the adiabatic regime (~ 760 °C) with a bimetallic OC (Fig. 2B) was lower compared to the monometallic one (800 °C [35]). Temperature depends on the rate and extent of oxidation reactions, while the higher AD_{exp} with bimetallic OCs implied better coupling between the exothermic oxidation and endothermic calcination. A similarly lower maximum temperature was also seen with hybrid materials combining CO_2 capture and oxygen transfer functionalities in one particle, which attained higher AD_{exp} than a mechanical mixture of CaO -based material and OC, due to the direct heat transfer and avoidance of conduction losses [34].

3.2.1. Effect of operating conditions in the calcination/oxidation stage

In an attempt to optimize the autothermicity achieved during the *calcination/oxidation stage*, a parametric study was conducted on the effect of oxidant type (air or pure O_2) and GHSV (Fig. 3). Experiments were carried out with the $\text{Ni}_{0.80}\text{Co}_{0.20}\text{-Zr}$ and the synthetic CaO -based

material (66 wt% $\text{CaO}/\text{CaZrO}_3$), by altering the gas feedstock while keeping a constant molar ratio of Ni-Co oxides to CaO of 0.5. Our previous work has shown that both parameters can affect the oxidation rate of the OC and the calcination driving force [36]. The latter is quantitatively defined as the difference between the equilibrium CO_2 partial pressure, which is a function of reaction temperature and the actual CO_2 partial pressure ($P_{\text{CO}_2,\text{eq}} - P_{\text{CO}_2}$) [42].

Gradual increase of the GHSV enhanced the AD_{exp} and decreased the duration of both regimes of *calcination/oxidation stage* (adiabatic and externally heated step, Fig. 3A). Higher GHSVs are associated with higher inlet flows of O_2 and thus faster completion of *calcination/oxidation stage*. The latter induces higher heat flux toward the carbonated CO_2 capture material, resulting in elevated AD_{exp} . The increasing flow of inert N_2 admitted to the reactor reduces the system's CO_2 partial pressure (P_{CO_2}), thus promoting the extent of the calcination reaction. The increase of GHSV did not affect the heat and mass transfer mechanisms or change significantly the ratios of thermal convection to conduction and mass convection to diffusion. This can be confirmed by calculating the Nusselt and Sherwood dimensionless numbers for different GHSVs (Fig. S2 in [Supplementary Material](#)) via empirical correlations [43].

In addition to the use of air, the operation of the *calcination/oxidation stage* was evaluated using pure O_2 as an oxidizing agent (Fig. 3B). The utilization of pure O_2 is an important prerequisite for the efficiency of the SE-CL-SMR process, since it allows the generation of a high-purity, ready for sequestration or downstream utilization CO_2 stream. The performance between air and O_2 flows under similar GHSV (500 h^{-1}) demonstrated that the autothermicity depends on the type of oxidant with higher AD_{exp} attained in pure O_2 (47.4% with O_2 compared to 40.6% with air). In addition, a notable decrease of the duration of the adiabatic operation regime (~ 4 min with O_2 compared to ~ 8 min with air) was also observed. Both are attributed to the higher partial pressure of O_2 and the highly accelerated OC re-oxidation. The absence of N_2 , which would acquire part of the heat released from the oxidation and prevent it from covering the calcination energy demand, is also beneficial. It should be noted that the absence of N_2 and the high consumption of inlet O_2 increase the partial pressure of desorbed CO_2 in the reactor. This implies that the temperatures of the bulk of solids were high enough to drive calcination despite the elevated CO_2 partial pressures.

Notwithstanding the positive effect of pure O_2 flow on the autothermicity degree attained, there was no notable change when further increasing the GHSV from 750 or 1000 h^{-1} . This was also observed in the case of using air as oxidant (Fig. 3A) with the higher GHSV values,

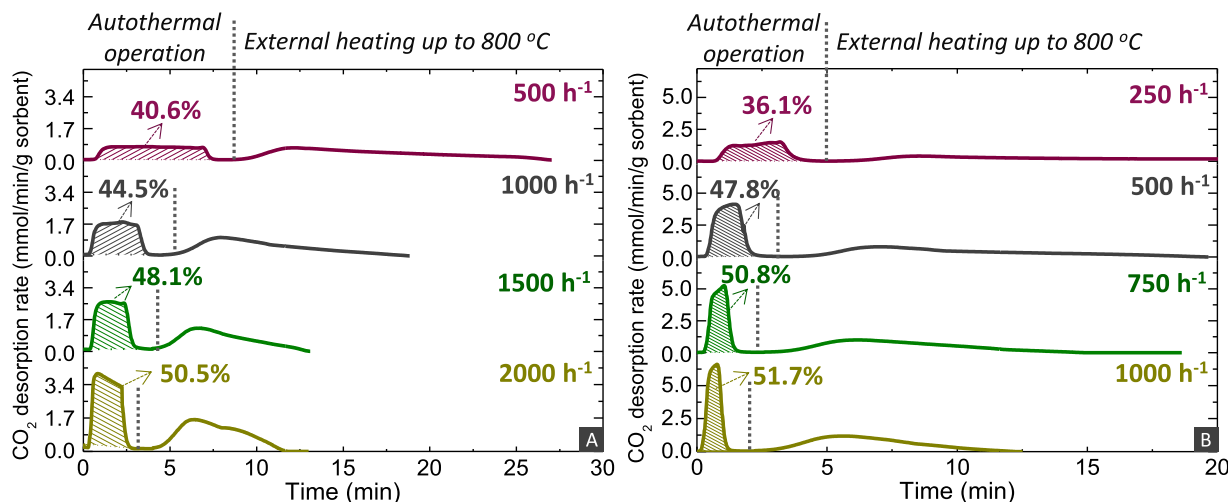


Fig. 3. CO_2 desorption rate versus time for different GHSVs when using (A) air and (B) O_2 as feed in the calcination/oxidation stage (reduction/reforming/carbonation stage: $T = 650$ °C, $\text{S/C} = 3$, $\text{GHSV} = 215 \text{ h}^{-1}$; calcination/oxidation stage: $T = 650 \rightarrow 800$ °C, molar $\text{Ni}_{0.80}\text{Co}_{0.20}\text{O}/\text{CaO} = 0.5$).

while the highest AD_{exp} attained with both gases was similar. Rough calculations of the theoretical autothermicity degree using a simplified expression (Eq. S5) of the [Supplementary Material](#) resulted in a value of ~62% for the operating conditions studied. This autothermicity upper limit was reached by ~84% with the use of pure O_2 at GHSV of 1000 h^{-1} . Considering that Eq. (S5) did not account for any heat losses from reactor walls or bypassing gas, the AD_{exp} attained was very close to the maximum realistic value under the conditions studied and thus highlights the efficient coupling between OC oxidation and $CaCO_3$ calcination.

Overall, the utilization of pure O_2 enables higher adiabatic calcination conversions compared to air, along with the co-generation of a highly concentrated CO_2 at the reactor exit. This operation, however, would increase the capital and operating cost due to required generation of pure O_2 from a costly air separation unit. The choice between air and pure O_2 oxidants relies on a detailed techno-economic assessment.

3.3. Cyclic stability

After completing the first cycle of SE-CL-SMR process, the same procedure was repeated for 22 cycles, corresponding to ~30 h of time on stream, to investigate the stability of materials. [Fig. 4A](#) illustrates the average H_2 purity and yield (after the end of OC reduction) attained in the *reduction/reforming/carbonation stage* over cycles in the presence of $Ni_{0.80}Co_{0.20}\text{-Zr}$ as OC. The material showed high stability in terms of both parameters, proving that the reduced Ni-Co maintains its catalytic activity for H_2 production (~0.98 mmol $H_2/\text{min/g}$ of reduced OC), despite being submitted in consecutive redox cycles. The CO_2 capture material also played a major role in the efficiency of H_2 producing stage. The material, which was the same as the one used in our previous studies [35,36], attained a 90% CaO conversion in the first cycle, followed by an almost negligible activity loss of 3% until the last cycle. The stable conversion can be also evidenced by the similar duration (~52.5 min) of the Pre-BT regime over cycles, which implies that the amount of H_2 produced is also retained stable during the cyclic operation. For the *calcination/oxidation stage* ([Fig. 4B](#)), after a slight reduction in the initial cycles, the AD_{exp} attained with $Ni_{0.80}Co_{0.20}\text{-Zr}$ when using air as oxidizing agent was stable. The monometallic oxygen carrier $Ni\text{-Zr}_{WI}$ presented satisfactory stability concerning the autothermicity degree, though constantly lower than that of the bimetallic OC. A cyclic experiment with pure O_2 was also carried out, with AD_{exp} slightly decreasing in the first cycles and tending to stabilize in the remaining operation, a behavior similar to the experiment with air.

3.4. Post-reaction characterization results

After the last *reduction/reforming/carbonation stage* of the 22-cycle SE-CL-SMR test, the CaO -based particles and the OC were easily separated from each other with the use of magnet, due to the magnetic properties of metallic Ni or Ni-Co alloys. The used $Ni_{0.80}Co_{0.20}\text{-Zr}$ was characterized in reduced and oxidized states to explore the changes in its physicochemical properties after cycling. The oxidized form was obtained by exposing the reduced OC after the separation of the two materials under air flow at $650\text{ }^\circ\text{C}$. As it was mentioned before, the CaO -based material, which has been extensively tested in our previous studies [35,36], attained stable conversion over cycles, which implies similar $CaCO_3$ amount at the beginning of all *calcination/oxidation stages* and the dependence of AD_{exp} mostly on the cyclic behaviour of the OC. Thus, this work focuses on characterizing exclusively the used OC to understand its contribution to AD_{exp} , while details on the used CO_2 capture material can be found elsewhere [35,36].

3.4.1. Exploring the role of Co in the coupling of oxidation and calcination

The aforementioned results highlighted the potential for more effective coupling of the OC oxidation and $CaCO_3$ calcination reactions. An explanation for this could lie on the different oxidation mechanism of bimetallic Ni-Co based materials, compared to their parent monometallic ones. Han et al. employed the environmental transmission electron microscopy to prove that these materials can form core-shell structures during oxidation that facilitate the reaction [44]. More specifically, following the formation of a thin oxide shell, metallic ions in the core diffuse outward to be oxidized according to the Kirkendall effect [45]. The Co ions segregate in the outer wall of the oxide shell and leave a Ni-rich layer on the inner shell wall. This leads to the formation of pinholes on the surface that subsequently facilitate the infiltration of oxygen molecules in the shell and the core, thereby enabling the more facile oxidation of the material compared to monometallic OCs. During the oxidation of monometallic Ni- or Co-based materials, the initially formed oxide shell is more conformal [46,47] and does not enable the infiltration of oxygen [44]. Performing XPS on the materials of this work showed that the $Co/(Co+Ni+Zr)$ ratio on the surface is nearly two times higher than the nominal bulk value (0.202 instead of 0.105) [40]. This proves the Co enrichment of the surface and supports that the OC may also undergo oxidation following similar mechanism.

In an attempt to study the oxidation behavior of the materials, the used OCs after the SE-CL-SMR experiments were subjected to oxidation at $650\text{ }^\circ\text{C}$, while monitoring the crystal structure alterations via *in-situ* XRD. [Fig. 5](#) displays the *in-situ* XRD patterns for the gradual oxidation

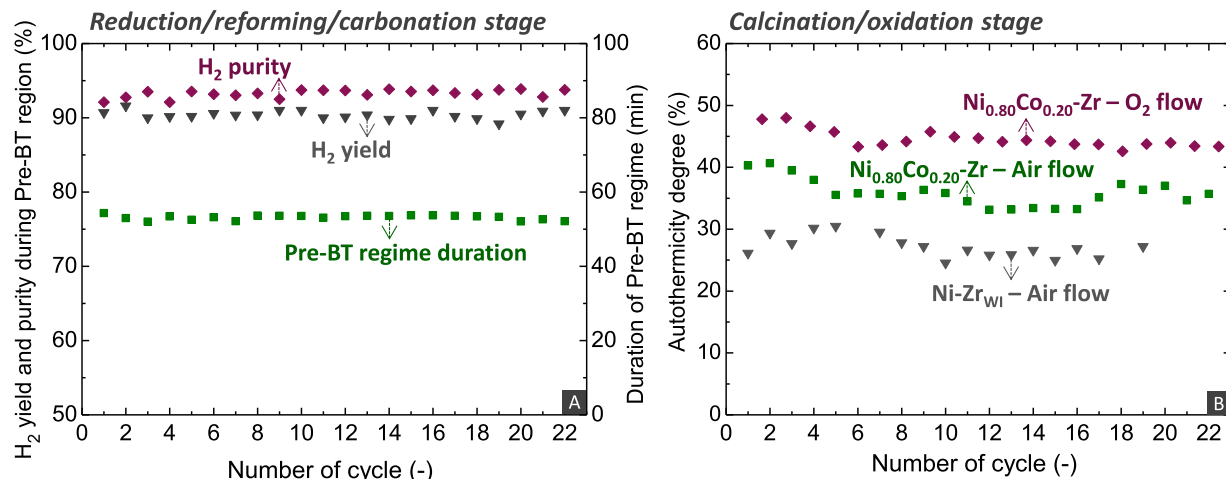


Fig. 4. (A) H_2 purity, yield and duration of Pre-BT regime using $Ni_{0.80}Co_{0.20}\text{-Zr}$ as OC and (B) AD_{exp} attained with bimetallic and monometallic OC over SE-CL-SMR cycles (reduction/reforming/carbonation stage: $T = 650\text{ }^\circ\text{C}$, $S/C = 3$, $GHSV = 215\text{ h}^{-1}$, molar $Ni_{(1-x)}Co_xO/CaO = 0.5$; calcination/oxidation stage: $T = 650 \rightarrow 800\text{ }^\circ\text{C}$, $GHSV = 430\text{ h}^{-1}$ for $Ni\text{-Zr}_{WI}$, $GHSV = 500\text{ h}^{-1}$ for $Ni_{0.80}Co_{0.20}\text{-Zr}$). Data of $Ni\text{-Zr}_{WI}$ is obtained from [35].

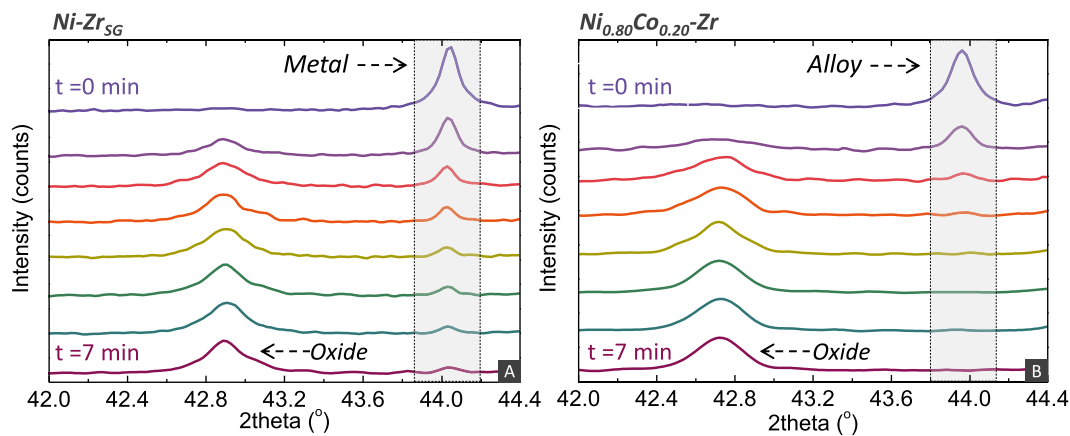


Fig. 5. In-situ XRD analysis of the reduced (A) Ni-Zr_{SG} and (B) Ni_{0.80}Co_{0.20}-Zr during re-oxidation at 650 °C under air atmosphere.

of the Ni-Zr and Ni_{0.80}Co_{0.20}-Zr materials. A single diffraction peak was initially visible in the 2θ range of 42–44° for both materials, which corresponds to either Ni metal or Ni-Co alloy. Since the measurements were performed at elevated temperatures, the diffraction peaks were shifted to lower 2θ values compared to their normal position at ambient conditions, because of the thermal lattice expansion. Furthermore, the peak corresponding to the Ni-Co alloy for the bimetallic OC was at lower 2θ values than the peak referring to metallic Ni in the monometallic material, since Co was inserted in the NiO lattice and provoked its expansion [48]. After exposing the materials to air, the intensity of the peak gradually decreased, while a second peak appeared at lower 2θ values, whose intensity increased over time. This change refers to the oxidation of the reduced OC and the formation of NiO or Ni-Co oxides in Ni-Zr and Ni_{0.80}Co_{0.20}-Zr respectively. However, Ni_{0.80}Co_{0.20}-Zr showed a faster decrease in the intensity of the peak corresponding to the Ni-Co alloy compared to the respective peak of the metallic Ni in Ni-Zr pointing to a different oxidation mechanism and a faster oxidation rate with Co addition. This result agrees with our previous work [40], which evaluated the redox kinetics of the studied OCs when tested under continuous redox cycles in TGA. A 4th order Avrami-Erofeev kinetic model fitted the oxidation stage of both bimetallic and monometallic OCs with high accuracy. A higher Arrhenius parameter was found for the bimetallic material, which relates to its faster oxidation kinetics [40].

It should be mentioned that Co addition could provoke two other effects, which might work in tandem with the higher oxygen infiltration and oxidation rate of the OC. The first is associated with the specific heat capacity of Co, which is nearly half of that of Ni (Table S1 of Supplementary Material). This implies that the substitution of Ni reduces the energy required for the heating of OC and thus increases the heat transferred to CaCO₃. The second effect is related to the nature of the oxides formed. As demonstrated from the Co_x-NiO_x phase diagram and the literature experimental data [44,49,50], thermal treatment under air at 650 °C enables the formation of both monoxide (e.g. Ni_xCo_{1-x}O) and spinel-type (e.g. Ni_xCo_{2-x}O₄) monometallic or bimetallic oxides, with the formation of the latter being more exothermic. This signifies that oxidation of a bimetallic OC may spontaneously release more energy compared to monometallic materials, which would be also beneficial for the AD_{exp} [44]. It would be expected though that both heat capacity and exothermicity are proportional to the Co content. This implies that their contribution to AD_{exp} is not as vital as the oxidation mechanism, since Ni_{0.88}Co_{0.12}-Zr and Ni_{0.80}Co_{0.20}-Zr attained similarly higher AD_{exp} compared to Ni-Zr_{WI} (Fig. 2 C), despite their different Co content. However, this statement does not exclude their potential contribution to AD_{exp} and future work could enlighten their role.

3.4.2. Evaluating the structure modifications of bimetallic OC

Determination of the crystal structure of the reduced material via ex-

situ XRD (Fig. 6A) revealed the complete reduction of the Ni-Co oxides and the formation of Ni-Co alloy phase. A common problem when testing materials for their reforming activity with excess steam (S/C=3) is related to the possible OC re-oxidation and loss of catalytic activity. However, this was avoided in the experiments of this work, due to the enhancing effect of in-situ CO₂ capture, which allows for higher H₂O consumption and H₂ production and thus a more reducing atmosphere in the reactor. No peaks of Ni-Co oxides were observed in the XRD pattern of the reduced OC, signifying an almost complete OC reduction even after 22 consecutive redox cycles. However, all peaks had higher intensity compared to respective peaks of the fresh reduced material, indicating larger crystallite sizes. This result was expected, given the OC exposure at elevated temperatures and the high content of active phase (40 wt%). In addition, it was found that the oxidation in pure O₂ or air flow affects sintering differently. In the experiment using O₂ as an oxidizing agent, the elevated temperatures in the bulk of the material rendered it vulnerable to sintering and to the formation of larger crystallite sizes. Indeed, the crystallite size of the Ni-Co alloy of the used OC showed a slightly more prominent growth (43.9 → 110.3 nm) compared to the experiment with air flow (43.9 → 96.9 nm). Sintering of OCs has been reported as a main consequence of consecutive redox cycles, while it can ultimately lead to the reduction of the catalytic activity of the reduced form of the material [35,51]. Nevertheless, the activity of the OC did not seem to be altered between cycles for the experiments with either of the two oxidants (Fig. 4), as a result of both the high weight fraction of Ni in the material and the high amount of OC in the reactor. Except from the active phase, diffraction peaks corresponding to ZrO₂ were also identified in the XRD patterns of used material, while it was observed that even though ZrO₂ was crystallized in monoclinic (m-ZrO₂) and tetragonal (t-ZrO₂) structures in the fresh material, t-ZrO₂ was absent in the reduced OC. This is can be attributed to the presence of steam in the reduction/reforming/carbonation stage, which is known to promote the transformation of t-ZrO₂ to m-ZrO₂ [52–54].

The XRD patterns of used oxidized OC (Fig. 6B) showed peaks referring to both Ni-Co oxides, while t-ZrO₂ re-appeared after the exposure under the oxidizing agent. The formation of t-ZrO₂ is possibly the result of the interaction of Co and Ni with ZrO₂, which allows for the reduction of oxygen vacancies upon exposure to the oxidizing agent [55]. The partial pressure of O₂ did not seem to affect the extent of t-ZrO₂ formation, given the similar intensity of t-ZrO₂ in the used OC XRD patterns obtained after oxidation with air and O₂.

The reducibility of the used oxidized OC retrieved after the SE-CL-SMR experiment with calcination performed with air as oxidizing agent was examined by employing TPR analysis. TPR profiles of fresh and used OCs (Fig. 7) exhibited two distinct H₂ consumption peaks, with the first (400–450 °C) referring to the reduction of Ni-Co oxides with low interaction to ZrO₂, while the peak at higher temperatures

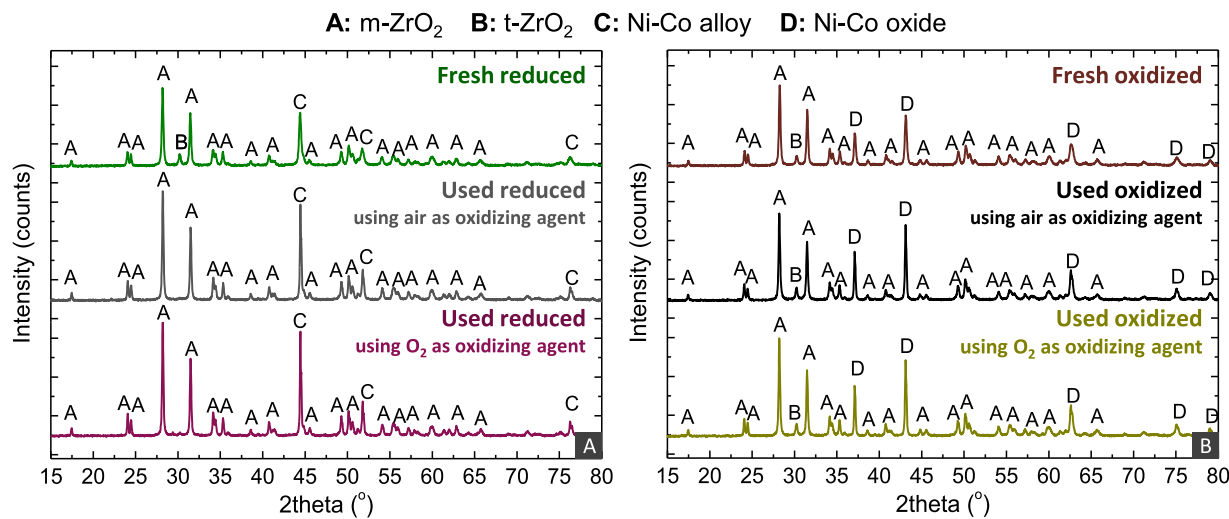


Fig. 6. XRD patterns of fresh and used $\text{Ni}_{0.80}\text{Co}_{0.20}\text{-Zr}$ oxygen carrier in (A) reduced and (B) oxidized state.

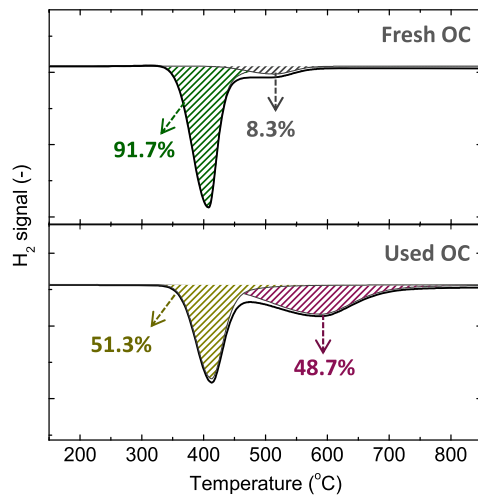


Fig. 7. H₂-TPR analysis of the fresh and used $\text{Ni}_{0.80}\text{Co}_{0.20}\text{-Zr}$ oxygen carrier.

(500–650 °C) corresponds to the reduction of oxides with stronger interaction with ZrO_2 [32]. Quantitative calculation of the consumed H₂ resulted in a similar degree of reduction for both materials, around 90–95%. Nonetheless, the ratio of the areas of strong/low interaction peaks was higher for the used oxidized OC compared to the fresh material. Moreover, the hydrogen consumption in the TPR profile of the used OC was completed at higher temperature (~675 °C) than the fresh material (~600 °C). Both results imply that the continuous redox cycles caused a reconstruction of the OC, which enables a stronger interaction between the Ni-Co oxides and the ZrO_2 . Another reason for the increase of the second peak area might be the agglomerated crystallites of the used Ni-Co oxides, which may hinder the H₂ diffusion and thus the reduction [33,56].

The oxidation behaviour of the used reduced OC from the SE-CL-SMR experiment where calcination was performed with air was tested via TPO analysis (Fig. 8). The signal acquired from TPO for the fresh OC displayed a broad O₂ consumption between 200 °C and 500 °C, composed of a main peak with maximum at ~425 °C and a small shoulder at ~300 °C. However, the TPO profile of the used OC demonstrated a single O₂ consumption peak with maximum at higher temperatures (~475 °C). Likewise with the alteration of the TPR profile between fresh and used OC, the changes in the TPO profile signify a different interaction between active and inert phases. Quantifying the

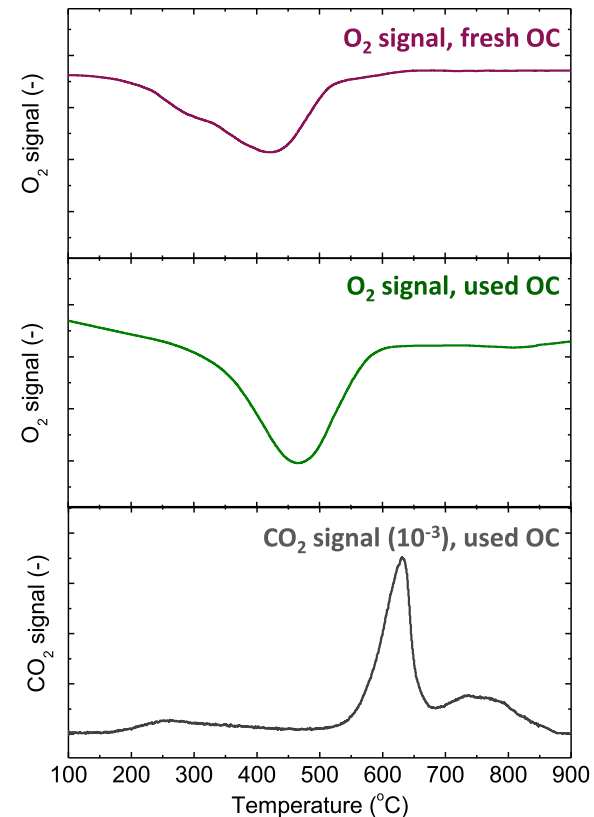


Fig. 8. TPO analysis of the fresh and used $\text{Ni}_{0.80}\text{Co}_{0.20}\text{-Zr}$ oxygen carrier.

consumption of O₂ revealed similar oxidation degree between fresh and used OC (92% and 87% respectively). Worthy to note, O₂ consumption was completed before reaching ~650 °C, the temperature in which the oxidizing agent is admitted for the *calcination/oxidation stage* of the SE-CL-SMR experiment.

The CO₂ signal evolution in the TPO profile of the used OC revealed three peaks for the oxidation of carbonaceous species formed in the *reduction/reforming/carbonation stage*. The first peak (200–250 °C) is related to adsorbed or amorphous carbon, the second peak (550–650 °C) corresponds to graphitic coke formed by CH₄ decomposition, while the third peak (675–850 °C) refers to another graphitic but less reactive

carbon, dissolved in bulk Ni [32,38,57]. Comparison of the position and the intensity of O_2 and CO_2 signals showed that the O_2 consumption does not coincide with the carbon oxidation, which indicates that the O_2 peak is ascribed almost exclusively to the OC re-oxidation and that the amount of coke deposited is very low. The latter was made possible by the quantification of the CO_2 released, resulting in less than 0.1 wt% solid carbon on the material, thereby proving the resistance to coke deposition. It should be mentioned that the CO_2 signal illustrated in Fig. 8 was obtained by multiplying the real signal with 10^3 for ease of reading.

XPS analysis was also performed to determine the alteration of the surface composition between fresh and used OCs. The deconvolution of signals is available in Fig. S3 of the *Supplementary Material*, while Fig. 9 compares the atomic composition of the surface of the fresh and used oxidized OCs, with the latter material been acquired from the SE-CL-SMR experiment where calcination was performed with air as oxidizing agent. For comparison, the bulk composition of the fresh OC ([40]) is also illustrated in the same figure. Even though Zr was homogeneously distributed on the surface and the bulk of the fresh OC, the Co content on the surface was higher compared to the nominal value at the expense of Ni. The enrichment of the surface with Co agrees with the aforementioned oxidation mechanism of the bimetallic material, according to which Co segregates at the outer wall of the oxide shell and forms pinholes that facilitate the oxidation of the core of material, ultimately leading to faster oxidation compared to the monometallic OC. For the used OC, it was found that Ni and Co contents on the surface decreased, implying their migration to the bulk of the material and interaction with ZrO_2 . This agrees with the shift of the H_2 and O_2 consumption peaks at higher temperatures in the TPR (Fig. 7) and TPO (Fig. 8) profiles respectively. All these structural changes and the enrichment of surface with ZrO_2 possibly affect the oxidation mechanism and may be related to the slight reduction of the AD_{exp} in the first cycles of the SE-CL-SMR experiment when using either air or O_2 (Fig. 4B).

Despite the decrease of the Ni and Co contents, the Ni/Co ratio on the surface was not altered between the fresh and the used OCs. Thus, the tendency of Co to migrate to the outer wall surface and provoke the oxidation mechanism which promotes the oxidation kinetics is retained with cyclic operation. This is probably the reason for the higher degrees of autothermicity compared to the ones attained with the monometallic Ni-based OC in the subsequent cycles. Ultimately, all aforementioned results and the attained steady operation highlight the suitability of the developed bimetallic OC for SE-CL-SMR.

4. Conclusions

This work focused on bimetallic Ni-Co oxides with ZrO_2 inert stabilizer as oxygen carriers for their performance in the sorption enhanced chemical looping steam methane reforming, along with their potential advantages compared to monometallic Ni-based materials. The evaluation was carried out via fixed bed reactor experiments using a mechanical mixture of the developed oxygen carriers and a $CaZrO_3$ -promoted CaO -based CO_2 sorbent. Operating synergistically with the CaO -based material in the reforming stage, the reduced bimetallic oxygen carrier had similar catalytic behavior as the monometallic ones, producing ~ 0.98 mmol H_2 /min/g of reduced OC with $\sim 94\%$ purity and $\sim 90\%$ yield at the relatively low reforming temperature of $650\text{ }^\circ C$. The addition of Co provided an alternative oxidation mechanism, which was beneficial for the re-oxidation rate of bimetallic materials. As a result, the oxidation of the bimetallic oxygen carrier attained 42% higher coverage of the calcination energy demand compared to a monometallic Ni-based oxygen carrier (40.6% autothermicity degree with bimetallic oxygen carrier compared to 28.6% with monometallic one) when applying a molar ratio of Ni-Co oxides to CaO equal to 0.5. The structure of the bimetallic oxygen carrier underwent a migration of Co and Ni to the bulk of the material, resulting to an increased interaction between

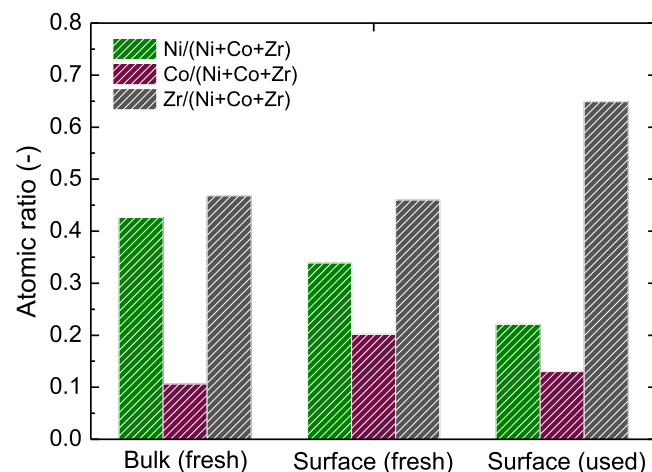


Fig. 9. Atomic composition of fresh and used $Ni_{0.80}Co_{0.20}\text{-Zr}$ oxygen carrier.

Co, Ni and ZrO_2 with consecutive redox cycles. Nevertheless, the succeeded autothermicity, along with the catalytic activity for high-purity H_2 generation displayed high stability in a 22-cycle operation. Using pure O_2 with a GHSV of $\sim 1000\text{ }h^{-1}$ it was possible to optimize the thermal coupling between calcination and oxidation and reach $\sim 84\%$ of the calculated maximum autothermicity degree. Overall, bimetallic Ni-Co oxygen carriers were proved as promising candidates for further reducing the energy demand of the intensified steam methane reforming process, thereby promoting its scalability in the future.

CRediT authorship contribution statement

Papalas Theodoros: Conceptualization, Formal analysis, Investigation, Methodology, Validation, Visualization, Writing – original draft. **Lemonidou Angeliki A.:** Resources, Supervision, Writing – review & editing. **Antzaras Andy:** Conceptualization, Supervision, Writing – review & editing.

Declaration of Competing Interest

The authors declare that they have no known competing financial interests or personal relationships that could have appeared to influence the work reported in this paper.

Data availability

Data will be made available on request.

Acknowledgments

The authors would like to thank Ms. Xanthi Ntampou from the Chemical Engineering Department of the Aristotle University of Thessaloniki in Greece for the XRD measurements. The authors also acknowledge the Laboratory of Advanced Materials and Devices (AMDe lab), School of Physics, for the access to the XPS/AES facilities of Large Research Infrastructure and Instrumentation of Aristotle University of Thessaloniki, Greece. Finally, Mr. Evangelos Palamas is also acknowledged for his contribution in performing part of the experimental work.

Appendix A. Supporting information

Supplementary data associated with this article can be found in the online version at doi:10.1016/j.apcatb.2024.123777.

References

- [1] S. van Renssen, The hydrogen solution? *Nat. Clim. Chang.* 10 (2020) 799–801, <https://doi.org/10.1038/s41558-020-0891-0>.
- [2] M.A. Rosen, S. Koohi-Fayegh, The prospects for hydrogen as an energy carrier: an overview of hydrogen energy and hydrogen energy systems, *Energy, Ecol. Environ.* 1 (2016) 10–29, <https://doi.org/10.1007/s40974-016-0005-z>.
- [3] IEA, Net zero by 2050: A roadmap for the global energy sector, 2021.
- [4] J.D. Holladay, J. Hu, D.L. King, Y. Wang, An overview of hydrogen production technologies, *Catal. Today* 139 (2009) 244–260, <https://doi.org/10.1016/j.cattod.2008.08.039>.
- [5] A.N. Antzaras, A.A. Lemonidou, Recent advances on materials and processes for intensified production of blue hydrogen, *Renew. Sustain. Energy Rev.* 155 (2022) 111917, <https://doi.org/10.1016/j.rser.2021.111917>.
- [6] H. Zhang, Z. Sun, Y.H. Hu, Steam reforming of methane: current states of catalyst design and process upgrading, *Renew. Sustain. Energy Rev.* 149 (2021) 111330, <https://doi.org/10.1016/j.rser.2021.111330>.
- [7] S.A. Bhat, J. Sadhukhan, Process intensification aspects for steam methane reforming: an overview, *AIChE J.* 55 (2009) 408–422, <https://doi.org/10.1002/aic.11687>.
- [8] D.P. Harrison, Sorption-enhanced hydrogen production: a review, *Ind. Eng. Chem. Res.* 47 (2008) 6486–6501, <https://doi.org/10.1021/ie800298z>.
- [9] C. Zhao, Z. Zhou, Z. Cheng, X. Fang, Sol-gel-derived, CaZrO_3 -stabilized $\text{Ni}/\text{CaO}-\text{CaZrO}_3$ bifunctional catalyst for sorption-enhanced steam methane reforming, *Appl. Catal. B Environ.* 196 (2016) 16–26, <https://doi.org/10.1016/j.apcatb.2016.05.021>.
- [10] A. Di Giuliano, K. Gallucci, Sorption enhanced steam methane reforming based on nickel and calcium looping: a review, *Chem. Eng. Process. Process. Intensif.* 130 (2018) 240–252, <https://doi.org/10.1016/j.cep.2018.06.021>.
- [11] B. Dou, C. Wang, Y. Song, H. Chen, B. Jiang, M. Yang, Y. Xu, Solid sorbents for in-situ CO_2 removal during sorption-enhanced steam reforming process: a review, *Renew. Sustain. Energy Rev.* 53 (2016) 536–546, <https://doi.org/10.1016/j.rser.2015.08.068>.
- [12] M. Shokrollahi Yancheshmeh, H.R. Radfarnia, M.C. Iliuta, High temperature CO_2 sorbents and their application for hydrogen production by sorption enhanced steam reforming process, *Chem. Eng. J.* (2016), <https://doi.org/10.1016/j.cej.2015.06.060>.
- [13] C. Ortiz, J.M. Valverde, R. Chacartegui, L.A. Perez-Maqueda, P. Giménez, The calcium-looping (CaCO_3/CaO) process for thermochemical energy storage in concentrating solar power plants, *Renew. Sustain. Energy Rev.* 113 (2019) 109252, <https://doi.org/10.1016/j.rser.2019.109252>.
- [14] L. Teng, Y. Xuan, Y. Da, X. Liu, Y. Ding, Modified Ca-looping materials for directly capturing solar energy and high-temperature storage, *Energy Storage Mater.* 25 (2020) 836–845, <https://doi.org/10.1016/j.ensm.2019.09.006>.
- [15] S.M. Kim, P.M. Abdala, M. Broda, D. Hosseini, C. Copéret, C. Müller, Integrated CO_2 capture and conversion as an efficient process for fuels from greenhouse gases, *ACS Catal.* 8 (2018) 2815–2823, <https://doi.org/10.1021/acscatal.7b03063>.
- [16] J. Hu, P. Hongnanorom, V.V. Galvita, Z. Li, S. Kawi, Bifunctional $\text{Ni}-\text{Ca}$ based material for integrated CO_2 capture and conversion via calcium-looping dry reforming, *Appl. Catal. B Environ.* 284 (2021) 119734, <https://doi.org/10.1016/j.apcatb.2020.119734>.
- [17] R.K. Lyon, J.A. Cole, Unmixed combustion: an alternative to fire, *Combust. Flame.* 121 (2000) 249–261, [https://doi.org/10.1016/S0010-2180\(99\)00136-4](https://doi.org/10.1016/S0010-2180(99)00136-4).
- [18] M. Rydén, P. Ramos, H_2 production with CO_2 capture by sorption enhanced chemical-looping reforming using NiO as oxygen carrier and CaO as CO_2 sorbent, *Fuel Process. Technol.* 96 (2012) 27–36, <https://doi.org/10.1016/j.fuproc.2011.12.009>.
- [19] A. Antzara, E. Heracleous, D.B. Bukur, A.A. Lemonidou, Thermodynamic analysis of hydrogen production via chemical looping steam methane reforming coupled with in situ CO_2 capture, *Int. J. Greenh. Gas. Control.* 32 (2015) 115–128, <https://doi.org/10.1016/j.egypro.2014.11.694>.
- [20] J. Powell, S. Wongsakulphasatch, R. Kokoo, N. Noppakun, C. Papainaianar, M.A. A. Aziz, S. Assabumrungrat, Optimisation of a sorption-enhanced chemical looping steam methane reforming process, *Chem. Eng. Res. Des.* 173 (2021) 183–192, <https://doi.org/10.1016/j.jcherd.2021.07.014>.
- [21] M.V. Navarro, J. Plou, J.M. López, G. Grasa, R. Murillo, Effect of oxidation-reduction cycles on steam-methane reforming kinetics over a nickel-based catalyst, *Int. J. Hydrog. Energy* 44 (2019) 12617–12627, <https://doi.org/10.1016/j.ijhydene.2018.12.056>.
- [22] S. Alam, J.P. Kumar, K.Y. Rani, C. Sumana, Self-sustained process scheme for high purity hydrogen production using sorption enhanced steam methane reforming coupled with chemical looping combustion, *J. Clean. Prod.* 162 (2017) 687–701, <https://doi.org/10.1016/j.jclepro.2017.05.136>.
- [23] J.R. Fernández, J.C. Abanades, Sorption enhanced reforming of methane combined with an iron oxide chemical loop for the production of hydrogen with CO_2 capture: conceptual design and operation strategy, *Appl. Therm. Eng.* 125 (2017) 811–822, <https://doi.org/10.1016/j.applthermeng.2017.07.063>.
- [24] Y. Yan, D. Thanganadar, P.T. Clough, S. Mukherjee, K. Patchigolla, V. Manovic, E. J. Anthony, Process simulations of blue hydrogen production by upgraded sorption enhanced steam methane reforming (SE-SMR) processes, *Energy Convers. Manag.* 222 (2020) 113144, <https://doi.org/10.1016/j.enconman.2020.113144>.
- [25] J.R. Fernández, J.C. Abanades, Reactor design for sorption-enhanced reforming using $\text{Ca}-\text{Cu}$ chemical loops, *Adv. Chem. Eng.* 51 (2017) 207–260, <https://doi.org/10.1016/bs.ache.2017.07.003>.
- [26] V. Dupont, A.B. Ross, I. Hanley, M.V. Twigg, Unmixed steam reforming of methane and sunflower oil: a single-reactor process for H_2 -rich gas, *Int. J. Hydrog. Energy* 32 (2007) 67–79, <https://doi.org/10.1016/j.ijhydene.2006.06.033>.
- [27] J. Fermoso, M.V. Gil, F. Rubiera, D. Chen, Multifunctional Pd/Ni-Co catalyst for hydrogen production by chemical looping coupled with steam reforming of acetic acid, *ChemSusChem* 7 (2014) 3063–3077, <https://doi.org/10.1002/cssc.201402675>.
- [28] B. Dou, Y. Song, C. Wang, H. Chen, M. Yang, Y. Xu, Hydrogen production by enhanced-sorption chemical looping steam reforming of glycerol in moving-bed reactors, *Appl. Energy* 130 (2014) 342–349, <https://doi.org/10.1016/j.apenergy.2014.05.061>.
- [29] O.A. Omoniyi, V. Dupont, Optimised cycling stability of sorption enhanced chemical looping steam reforming of acetic acid in a packed bed reactor, *Appl. Catal. B Environ.* 242 (2019) 397–409, <https://doi.org/10.1016/j.apcatb.2018.09.083>.
- [30] T. Papalas, A.N. Antzaras, A.A. Lemonidou, Intensified steam methane reforming coupled with Ca-Ni looping in a dual fluidized bed reactor system: a conceptual design, *Chem. Eng. J.* 382 (2020) 122993, <https://doi.org/10.1016/j.cej.2019.122993>.
- [31] A. Antzara, E. Heracleous, A.A. Lemonidou, Improving the stability of synthetic CaO -based CO_2 sorbents by structural promoters, *Appl. Energy* 156 (2015) 331–343, <https://doi.org/10.1016/j.apenergy.2015.07.026>.
- [32] A. Antzara, E. Heracleous, L. Silvester, D.B. Bukur, A.A. Lemonidou, Activity study of NiO -based oxygen carriers in chemical looping steam methane reforming, *Catal. Today* 272 (2016) 32–41, <https://doi.org/10.1016/j.cattod.2015.10.027>.
- [33] L. Silvester, D. Ipsakis, A. Antzara, E. Heracleous, A.A. Lemonidou, D.B. Bukur, Development of NiO -based oxygen carrier materials: effect of support on redox behavior and carbon deposition in methane, *Energy Fuels* 30 (2016) 8597–8612, <https://doi.org/10.1021/acs.energyfuels.6b01520>.
- [34] A.N. Antzaras, E. Heracleous, A.A. Lemonidou, Hybrid catalytic materials with CO_2 capture and oxygen transfer functionalities for high-purity H_2 production, *Catal. Today* 369 (2021) 2–11, <https://doi.org/10.1016/j.cattod.2020.06.018>.
- [35] A. Antzara, E. Heracleous, A.A. Lemonidou, Energy efficient sorption enhanced-chemical looping methane reforming process for high-purity H_2 production: experimental proof-of-concept, *Appl. Energy* 180 (2016) 457–471, <https://doi.org/10.1016/j.apenergy.2016.08.005>.
- [36] A.N. Antzaras, E. Heracleous, A.A. Lemonidou, Sorption enhanced-chemical looping steam methane reforming: optimizing the thermal coupling of regeneration in a fixed bed reactor, *Fuel Process. Technol.* 208 (2020) 106513, <https://doi.org/10.1016/j.fuproc.2020.106513>.
- [37] M.M. Tijani, A. Aqsha, N. Yu, N. Mahinpey, Determination of redox pathways of supported bimetallic oxygen carriers in a methane fuelled chemical looping combustion system, *Fuel* 233 (2018) 133–145, <https://doi.org/10.1016/j.fuel.2018.06.017>.
- [38] M. Torimoto, Y. Sekine, Effects of alloying for steam or dry reforming of methane: a review of recent studies, *Catal. Sci. Technol.* 12 (2022) 3387–3411, <https://doi.org/10.1039/d2cy00066k>.
- [39] X. Zhang, K. Yim, J. Kim, D. Wu, S. Ha, Elucidating the promoting role of Mo_2C in methane activation using $\text{Ni}-\text{xMo}_2\text{C}/\text{FAU}$ to catalyze methane steam reforming, *Appl. Catal. B Environ.* 310 (2022), <https://doi.org/10.1016/j.apcatb.2022.121250>.
- [40] T. Papalas, E. Palamas, A.N. Antzaras, A.A. Lemonidou, Evaluating bimetallic $\text{Ni}-\text{Co}$ oxygen carriers for their redox behavior and catalytic activity toward steam methane reforming, *Fuel* 359 (2024) 130272.
- [41] S.Z. Abbas, V. Dupont, T. Mahmud, Modelling of high purity H_2 production via sorption enhanced chemical looping steam reforming of methane in a packed bed reactor, *Fuel* 202 (2017) 271–286, <https://doi.org/10.1016/j.fuel.2017.03.072>.
- [42] A. Scaltsyrianne, A. Lemonidou, CaCO_3 decomposition for calcium-looping applications: Kinetic modeling in a fixed-bed reactor, *Chem. Eng. Sci. X* 8 (2020) 100071, <https://doi.org/10.1016/j.cesx.2020.100071>.
- [43] W. Ranz, W. Marshall, Evaporation from drops, *Chem. Eng. Prog.* 48 (1952) 173–180, 141–146.
- [44] L. Han, Q. Meng, D. Wang, Y. Zhu, J. Wang, X. Du, E.A. Stach, H.L. Xin, Interrogation of bimetallic particle oxidation in three dimensions at the nanoscale, *Nat. Commun.* 7 (2016) 1–9, <https://doi.org/10.1038/ncomms13335>.
- [45] Y. Yin, R.M. Rioux, C.K. Erdonmez, S. Hughes, G.A. Somorjai, A.P. Alivisatos, Formation of hollow nanocrystals through the nanoscale Kirkendall effect, *Science* 304 (2004) 711–714, <https://doi.org/10.1126/science.1096566>.
- [46] J.G. Railsback, A.C. Johnston-Peck, J. Wang, J.B. Tracy, Size-dependent nanoscale Kirkendall nanoparticles, *ACS Nano* 4 (2010) 1913–1920, <https://doi.org/10.1021/nn901736y>.
- [47] Z. Yang, N. Yang, J. Yang, J. Bergström, M.P. Pilani, Control of the oxygen and cobalt atoms diffusion through Co nanoparticles differing by their crystalline structure and size, *Adv. Funct. Mater.* 25 (2015) 891–897, <https://doi.org/10.1002/adfm.201403617>.
- [48] Z. Sun, W. Shi, C. Pei, C.K. Russell, D. Cheng, Z. Sun, J. Gong, Tailoring lattice oxygen triggered $\text{NiO}/\text{Ca}_9\text{Co}_{12}\text{O}_{28}$ catalysts for sorption-enhanced renewable hydrogen production, *Appl. Catal. B Environ.* 316 (2022) 121642, <https://doi.org/10.1016/j.apcatb.2022.121642>.
- [49] S. Kuboon, Y.H. Hu, Study of $\text{NiO}-\text{CoO}$ and $\text{Co}_3\text{O}_4-\text{Ni}_3\text{O}_4$ solid solutions in multiphase $\text{Ni}-\text{Co}-\text{O}$ systems, *Ind. Eng. Chem. Res.* 50 (2011) 2015–2020, <https://doi.org/10.1021/ie101249r>.
- [50] J. Robin, Constitution and stability of several solids solutions based on cobalt oxide, *Ann. Chim.* 10 (1955) 389–412.
- [51] M.V. Navarro, J.M. López, T. García, G. Grasa, R. Murillo, Catalyst evaluation for high-purity H_2 production by sorption-enhanced steam-methane reforming

coupled to a Ca/Cu process, *J. Power Sources* 363 (2017) 117–125, <https://doi.org/10.1016/j.jpowsour.2017.07.075>.

[52] S. Xie, E. Iglesia, A.T. Bell, Water-assisted tetragonal-to-monoclinic phase transformation of ZrO_2 at low temperatures, *Chem. Mater.* 12 (2000) 2442–2447, <https://doi.org/10.1021/cm000212v>.

[53] H. Wang, G. Li, Y. Xue, L. Li, Hydrated surface structure and its impacts on the stabilization of t- ZrO_2 , *J. Solid State Chem.* 180 (2007) 2790–2797, <https://doi.org/10.1016/j.jssc.2007.08.015>.

[54] E.M. Köck, M. Kogler, T. Götsch, L. Schlicker, M.F. Bekheet, A. Doran, A. Gurlo, B. Klötzer, B. Petermüller, D. Schildhammer, N. Yigit, S. Penner, Surface chemistry of pure tetragonal ZrO_2 and gas-phase dependence of the tetragonal-to-monoclinic ZrO_2 transformation, *Dalt. Trans.* 46 (2017) 4554–4570, <https://doi.org/10.1039/c6dt04847a>.

[55] J. Chevalier, L. Gremillard, A.V. Virkar, D.R. Clarke, The tetragonal-monoclinic transformation in zirconia: Lessons learned and future trends, *J. Am. Ceram. Soc.* 92 (2009) 1901–1920, <https://doi.org/10.1111/j.1551-2916.2009.03278.x>.

[56] Z. Li, X. Hu, L. Zhang, S. Liu, G. Lu, Steam reforming of acetic acid over Ni/ ZrO_2 catalysts: effects of nickel loading and particle size on product distribution and coke formation, *Appl. Catal. A Gen.* 417–418 (2012) 281–289, <https://doi.org/10.1016/j.apcata.2012.01.002>.

[57] T. Skalar, E. Jelen, B. Novosel, M. Marinšek, Oxidation of carbon deposits on anode material Ni–YSZ in solid oxide fuel cells, *J. Therm. Anal. Calorim.* 127 (2017) 265–271, <https://doi.org/10.1007/s10973-016-5671-8>.